Geomechanics and Engineering, *Vol. 26, No. 2 (2021) 205-214*
https://doi.org/10.12989/gae.2021.26.2.205

Effect of underground stress transfer through artificial manipulation of particle size distribution

Zhen-Hua Xin[1a], Jun-Ho Moon[3b], Kab-Boo Kim[2c], Chan-Hee Kim[3d] and Young-Uk Kim*[3]

[1]*Department of Infrastructure Safety Research, KICT, Goyang 10223, Korea*
[2]*Bosiddol Inc., Nonhyeon-ro 63, Gangnam-gu, Seoul, 06256, Korea*
[3]*Department of Civil Engineering, Myongji University, Yongin 17058, Korea*

(Received December 18, 2020, Revised April 26, 2021, Accepted July 13, 2021)

Abstract. To maintain the stability of built structures, engineers employ various methods to increase ground strength. One such method is to exert mutual physical force upon a structure, thereby stabilizing it without external reinforcement. Typical examples include the stone mastic asphalt method and torsional structured stonework. By simulating a structural phenomenon, it is possible to increase the ground's strength simply by manipulating the distribution and spatial arrangement of soil particles; soil composed of two differently sized particles satisfying a specific ratio does not separate easily. The jamming of soil particles utilizes Plato's regular polyhedron model and assumes that soil particles are complete spheres. Larger soil particles are placed at each vertex of a regular polyhedron and smaller particles in the voids' center. All soil particles come into contact with each other, thereby inducing an interlocking effect. When applied to soil, the particle size distribution is found to be gap-graded. This study investigates this mechanism by using numerical analysis and centrifuge tests to initiate the interlocking effect by distributing gap-graded particles and conducting plate-load tests to verify the ground reinforcement effect.

Keywords: gap-graded soil; ground reinforcement; interlocking; particle; particle size distribution; replacement method

1. Introduction

There are many physical, chemical, and electrical methods for improving soft ground with poor engineering characteristics. Among these, physical improvement methods are widely applied considering economic efficiency, technical level, and environmental pollution. Main physical improvement methods for cohesive soil include pre-loading, vertical drainage, geotextile reinforcement, and grouting. Pre-loading is one of the oldest and most widely used physical improvement methods. It is effective and economical but requires a very long construction period. In the case of thick clay layers with poor water permeability, it is necessary to use vertical drainage or geotextile reinforcement method to shorten the construction period (Saride *et al*. 2013). On the other hand, it is economically inefficient because of the complexity of construction and the demand for design.

Grouting is a method for increasing the strength and impermeability of soil by inserting a tube into the ground and injecting appropriate amounts of chemical liquid (injectable material) under pressure to solidify or harden it. This injection method is simple to prepare and install and can be implemented in narrow places. It has little effect on vibration and noise over a short period; however, there is a problem with heavy metals such as Cr6+ flowing into rivers with rainwater. The purpose of improving the soft ground while taking these economic and environmental problems into account is to solve the structural stability problems caused by low soil strength and bearing capacities. Various studies have been conducted to increase soil's internal strength by exerting joint physical forces without reinforcement from the outside (Cho *et al*. 2006, Oda 1977, Takao *et al*. 2006). According to Takao's (2011) study, the shear resistance angle increases even with small amounts of sand when gravel is added. Yagiz (2001) showed that the shear resistance angle was largest when the soil was mixed with over 20% sand in the shear resistance test. Yagiz's study shows that the interlocking effect of the mixed gravel is better.

Taiwan suffers from aggregate shortages because 90% of its roads are built with asphalt and aggregate pavements. Therefore, Shen (2005) evaluated the performance of asphalt pavement using gap-graded aggregate gradation to improve the aggregate utilization efficiency. Under this method, increasing the object's contact area increases the aggregate density to the point that it becomes solid. This physical process is called jamming (Siemens *et al*. 2010, Vallejo *et al*. 2009). Jamming phenomena are related to the particle size distribution and size shape; in general, when

*Corresponding author, Professor
E-mail: yukim@mju.ac.kr
[a]Ph.D.
E-mail: hua97@naver.com
[b]Research Professor
E-mail: jhmoon@mju.ac.kr
[c]CEO
E-mail: kgbsns@daum.net
[d]Master Student
E-mail: 3757x@naver.com

ISSN: 2005-307X (Print), 2092-6219 (Online)

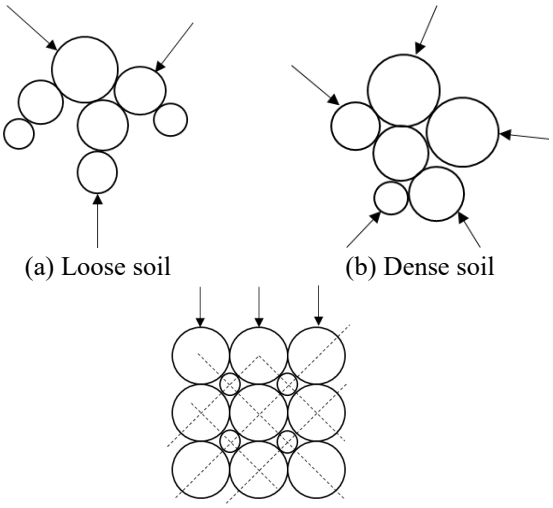

(a) Loose soil (b) Dense soil

(c) Gap-graded soil

Fig. 1 Evaluation of particle overlapping

this distribution varies, the bearing capacity is improved (Alias *et al*. 2014, Kamura *et al*. 2016). However, few studies have shown the jamming effect of improving the bearing capacity for gap granularity. The gap-graded condition refers to an artificially manipulated particle size distribution that generates frictional resistance between the surfaces and causes a horizontal restraining force according to the load, thereby causing lateral jamming through frictional resistance of the surfaces. If sufficient consideration is made of the particle size distribution and support capacity, a strong ground can be created even if the sized particles are not diverse.

2. Theoretical background of the gap-graded particle distribution

As shown in Fig. 1, loose soil has a low contact frequency between particles when the upper force is applied because the contact points between particles transfer mostly vertical compression forces. On the other hand, dense soil has high frictional resistance due to numerous contact points transferring vertical and horizontal compression forces, with the latter generating friction. Soils formed with a gap-graded granularity develop well-structured contact points between particle layers. When a vertical compressive force is applied, the contact frequency between particles is high, and the best frictional resistance is generated by the systematic contact forces acting in the horizontal direction. Filling the central space systematically with polyhedrons leads to a hierarchical structure in any direction, which increases the rigidity of particle materials.

In other words, the rigid base of the hierarchical structure generates a horizontal restraining force when a vertical force is applied and causes horizontal deformation of the soil particles. The concept of gap-sized particle has widely been used in related studies on asphalt pavements. This size is defined as the particle size distribution with one or more intermediate grades omitted (Shen 2005). In this study, gap-graded particle distribution applied to the ground

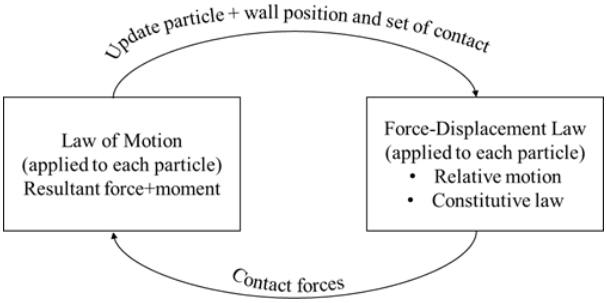

Fig. 2 Calculation cycle in PFC2D (Itasca 1999)

is defined as the particle size ratio between the large and small aggregates between 1.1 and 4.45. The composition ratio of the aggregate used in the tests was calculated according to several principles. The center of a large particle is located at the corner of the regular polyhedron and the smaller particle is at the center of the regular polyhedron. The composition ratio of small particles to large particles in the sample was assumed to be 1:1 by expanding infinitely the arrangement of particles in a regular polyhedron (Xin *et al*. 2016). Since the specific gravity is assumed to be the same, the volumetric ratio corresponds to the weight ratio. Thus, the composition ratio of the gap-graded soil can be obtained as in Eq. (1).

$$W_{big} = V_{big} = \frac{R^3}{R^3 + r^3}$$

$$W_{small} = V_{small} = \frac{r^3}{R^3 + r^3}$$

R: Big particle diameter

r: Small particle diameter

W_{big}: Big particle weight ratio

V_{big}: Big particle volumetric ratio

W_{small}: Small particle weight ratio

V_{small}: Small particle volumetric ratio (1)

3. Effect of particle size distribution on stress through numerical analysis

3.1 Particle Flow Code (PFC)

The Particle Flow Code (PFC) is a general purpose, distinct element modeling (DEM) framework. The PFC models synthetic materials composed of an assembly of variably sized rigid particles that interact at contacts to represent both granular and solid materials. The PFC models simulate the independent movement (translation and rotation) and interaction of many rigid particles that may interact at contact interfaces based on an internal force and moment. The calculation cycle in the particle flow code 2D (PFC2D) is a time-stepping algorithm that requires the repeated application of the law of motion to each particle, a force-displacement law to each contact, and a constant updating of wall positions. Contacts, which may exist between two balls or between a ball and a wall, are formed and broken automatically during a simulation. The

Table 1 Gap-sized particles and homogeneous particle conditions

Large sieve (mm)	Small sieve (mm)	Average particle size (mm)	m								
			1	2	3	4	5	6	7	8	9
8	6.7	7.35	1.13	1.23	1.42	1.68	2.00	2.39	2.85	3.37	3.97
6.7	6.35	6.525	1.09	1.26	1.49	1.78	2.12	2.53	2.99	3.53	4.21
6.35	5.6	5.975	1.15	1.37	1.63	1.94	2.32	2.74	3.23	3.85	
5.6	4.75	5.175	1.18	1.41	1.68	2.01	2.37	2.80	3.34		
4.75	4	4.375	1.19	1.42	1.70	2.01	2.36	2.82			
4	3.35	3.675	1.20	1.42	1.69	1.99	2.37				
3.35	2.8	3.075	1.19	1.41	1.66	1.98					
2.8	2.36	2.58	1.18	1.39	1.66						
2.36	2	2.18	1.18	1.41							
2	1.7	1.85	1.19								
1.7	1.4	1.55									

Table 2 Multi-sized particle distributions

Particle size (mm)	Volume ratio (%)	Uniformity coefficient (C_u)	Coefficient of curvature (C_C)
0.5	0.21		
1.5	3.02		
1.9	21.88		
3.5	0.42		
4.75	1.88	3.95	2.20
5.6	3.33		
6.5	20.83		
7.5	8.33		
8.5	40.1		

calculation cycle is illustrated in Fig. 2. At the start of each timestep, the set of contacts is updated from the known particle and wall positions. The force-displacement law is then applied to each contact to update the contact forces based on the relative motion between the two entities at the contact and the contact constitutive model. Next, the law of motion is applied to each particle to update its velocity and position based on the resultant force and moment arising from the contact forces and anybody forces acting on the particle. Also, the wall positions are updated based on the specified wall velocities. The calculations performed in each of the two boxes of Fig. 2 can be done effectively in parallel.

3.2 Uniaxial-compression simulation

Theoretically, if the ground's particle size distribution consisted of body-centric polyhedrons, small particles should fit perfectly like puzzle pieces between large particles. However, it is almost impossible to arrange soil particles in such a fashion without using large masses such as rocks. Therefore, the specimens' particle size and compounding ratio according to a theoretical formula, and particles were generated and distributed randomly. This study aims to find and verify the particle size distribution that causes the interlocking effect through numerical analysis (Nikadat *et al*. 2016, Wang *et al*. 2014). Three conditions were considered in numerical analysis and experiment conditions: a homogeneous particle size, gap-graded particle size, and multi-particle size. As shown in Table 1, the homogeneous particles have 11 different sizes

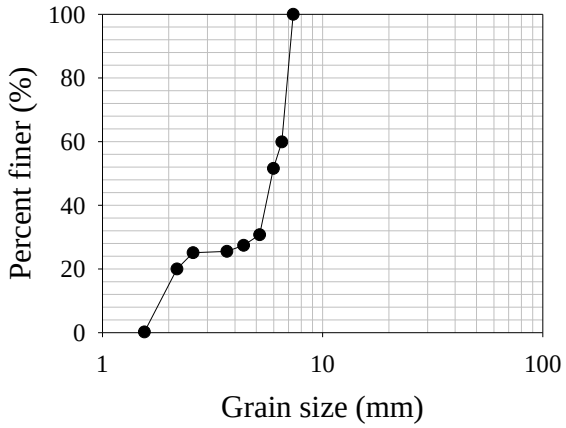

Fig. 3 Grading size distribution curve

between 1.55 and 7.35 mm. The gap-graded condition was composed by combining particles of 11 different sizes into two groups of large-sized and small-sized particles (m=R/r). The gap-graded condition value m contains 54 particle sizes ranging between 1.09 and 4.21. As shown in Table 2, the multi-sized particle condition was composed by combining particles of 9 different sizes. The uniformity coefficient (Cu) is 3.95, and the coefficient of curvature (C_C) is 2.20. It is close to a well-graded condition but not a smooth curve distribution with nine differently sized particles artificially manipulated (Fig. 3).

The uniaxial compression numerical analysis conditions are shown in Fig. 4, and the particle distributions are shown by colors. The condition of a single color, as in Fig. 4(a), is

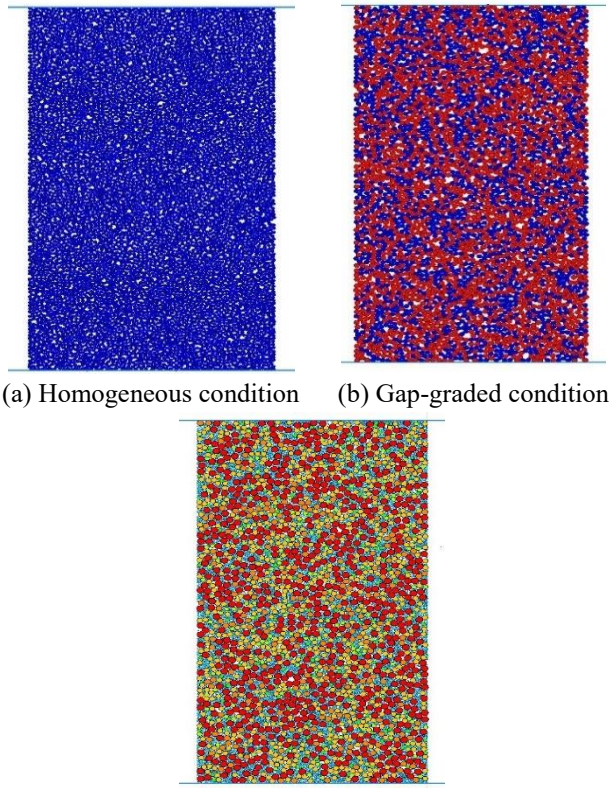

(a) Homogeneous condition (b) Gap-graded condition

(c) Gap-graded soil

Fig. 4 Uniaxial compression simulation analysis results

Table 3 Particle properties

Properties	Value
Parallel bond normal strength, σ_c	100 MPa
Parallel bond shear strength, τ_c	100 MPa
Slip coefficient of ball-ball	0.577
Ball density	2000 kg/m^3
Damping coefficient	0.2
Void ratio	0.1
Young's modulus, GPa	40.0
Speed of boundary wall	0.1 m/min
Particle normal/shear stiffness, Kn/Ks	2.5
Parallel bond normal/shear stiffness, Kn/Ks	3.0
Poisson's ratio, λ	0.25

a homogeneous particle distribution. In Fig. 4(b), red indicates large-sized particles and blue small-sized particles under the gap-graded condition. Fig. 4(c) shows a multi-sized particle distribution composed of nine differently sized particles. The particles' properties are shown in Table 3; the boundary is 50 × 100 cm and is randomly generated in the bounding box according to the particle size and ratio of particles with a pore ratio of 0.1. After the granular specimen with the calculated ratio was created, the boundary between the two sides disappeared. The boundary wall moved from the upper level to the lower level at the 1 cm/min speed to load the specimen. The boundary wall continued to move until the compressive load reached 70% above the ultimate capacity, at which point it stopped.

From Fig. 5, the uniaxial compressive strength is much higher in the gap-graded condition than in the multi-sized

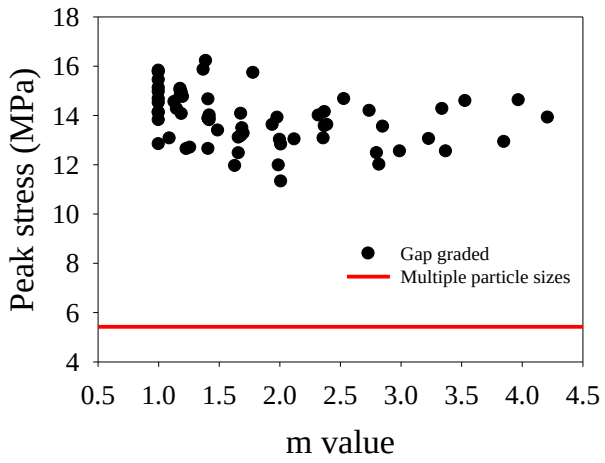

Fig. 5 Uniaxial compression strength according to the particle size distribution

particle conditions. According to numerical analysis, the maximum uniaxial compressive strength of the specimen consisting of multi-sized particles is 5.42 MPa, and the maximum uniaxial compressive strength is 16.2 MPa. The particle size compositions showing the maximum uniaxial compressive strengths are 7.35 and 5.175 mm, and the gap-graded particle size ratio is m=1.42. By comparison, it can be seen that the gap-graded particle with high uniaxial compressive strength is between m=1 and m=1.5

3.3 Simulation of underground stress transfer in upper structures

The gap-graded particle size samples included 54 cases of the ratio m=R/r of large to small particles of between 1.09 and 4.21 composed of 11 particle sizes, similar to uniaxial compression simulation. The simulation model is shown in Fig. 6(a). The size of the ground model is 23 m × 17 m. The ground is composed of two layers: the general support layer and the substitution ground, with depths of 2 m and 7 m. This sequence will create a view, which we have called "Contact Force," and make it the current view. The forces that develop between ball contacts are plotted as lines with thickness proportional to force magnitude. The contact forces are added to the plot of balls and walls, as shown in Fig. 6(b). The support layer is homogeneous with a particle size of 8.5 mm. The substitution ground was simulated with different conditions, i.e., multi-sizes particles, homogeneously sized particles, and particles with gap-graded sizes. The particle properties and multi-sized particle distribution was the same as the uniaxial compression simulation. The superstructure was 5 m × 10 m in size, and the strata were formed and travelled at 15 cm/s. The superstructure was rigid and moved in the direction of gravity at a constant speed without being affected by the bearing force. The underground stress values transmitted from the middle position of the lower ground to the marked circular plot position were monitored until the convergence state. The ground stress value is the average value of the stress over the plot area.

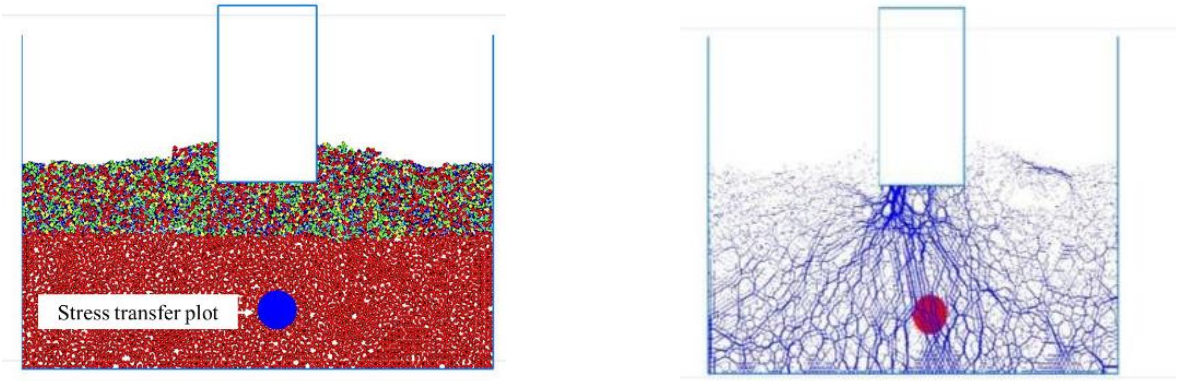

(a) Ground composition of numerical simulation (b) Underground stress distribution

Fig. 6 Underground stress distribution simulation

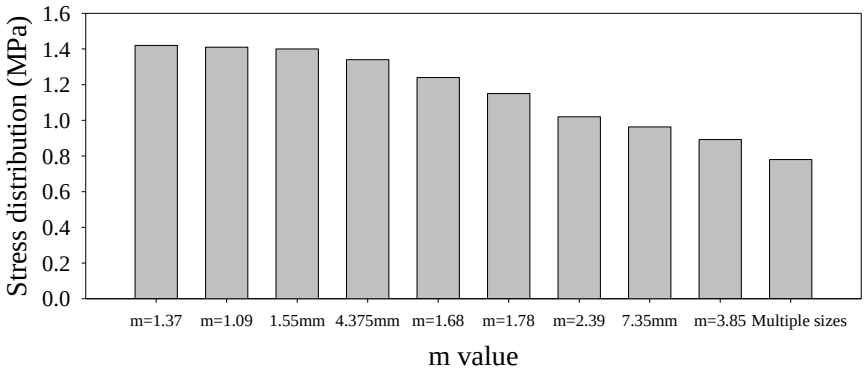

Fig. 7 Ground stress distribution of upper structures

From Fig. 7, the stress dispersion effect was the highest at m=1.37, followed by the homogeneous particle size, while the lowest stress dispersion effect was for the multi-sized particle condition. From the numerical results, it is determined that the reduction of ground stress distribution can be up to two times higher than in the multi-sized particle condition when certain gap-graded size conditions are satisfied. If the proportion of small particles that act as a keystone is very small among randomly distributed sizes, the probability of producing an interlocking effect will be relatively small. Therefore, additional verification will be conducted through experiments, comparing the results with the gap-graded condition that exhibited high strength.

4. Experiment method and results

4.1 Finding optimum gap-graded condition through centrifugal model tests

4.1.1 Centrifugal model tester

The centrifugal model tests were performed to evaluate the ground stress distribution caused by a structure placed on the soft ground. The tester had two 100 cm rotating arms attached symmetrically and was able to apply rotational centrifugal force up to 150 g gravitational acceleration with a motor capacity of 10.0 HP. The cross-sectional view of the centrifugal model tester is shown in Fig. 8 below. The standing structure was 155 mm × 155 mm × 130 mm in length, width, and height, and the strain box was filled with iron beads and weighing 12.5 kg. For scaling the structure at a ratio of 67:1, a centrifugal force of 67 times that of gravity was applied. In the centrifugal model test, the scaling factor was based on the size of aggregate particles actually used. The stress distribution in the soft ground was thus observed in similar conditions to those that occur for real structures and soils. In the centrifugal model test, the standing structure's stress applied to the ground is 256.6 kPa.

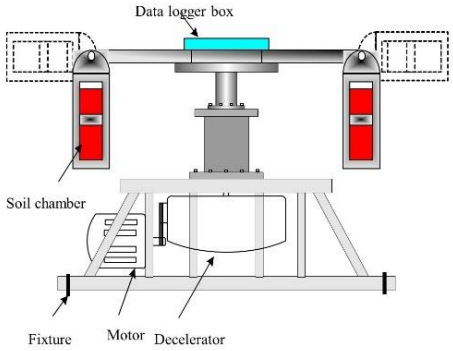

Fig. 8 Centrifugal model tester

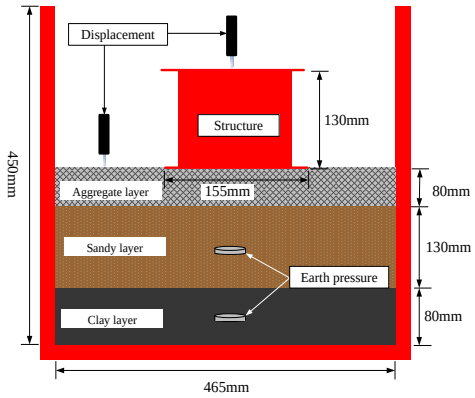

Fig. 9 Cross-section of centrifugal model chamber

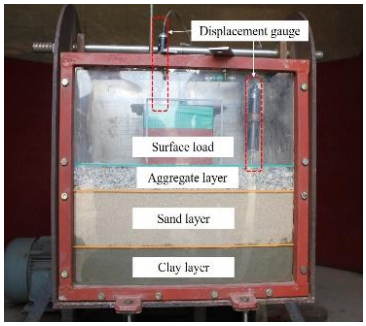

(a) Ground layer composition

(b) Earth pressure gauge

Fig. 10 Centrifugal model experiment setting

4.1.2 Centrifugal model structure and ground composition

The centrifugal model structure and ground composition are shown in Figs. 9 and 10. The centrifuge chamber's internal dimensions were 46 cm long, 25 cm wide, and 45 cm deep. The lower part of the chamber was filled with 8 cm of clay to form the soft ground and then filled with the Jumunjin standard sand to a height 13 cm above the clay. Finally, an 8 cm deep silica sand substituted layer was formed above the sandy ground. After the clay layer and the sandy soil layer were stacked, the ground was compacted with the same energy. Before substituting silica sand ground, silica sand was washed with water and dried in an oven to remove small fine particles. The dried silica sand was subjected to sieve analysis to obtain specific particles of silica sand. The particle distribution in the silica sand layer was manipulated based on the ratio m of small sized to large sized particles, and the weight was set to 10 kg per case. Earth pressure gauges were installed in the middle of

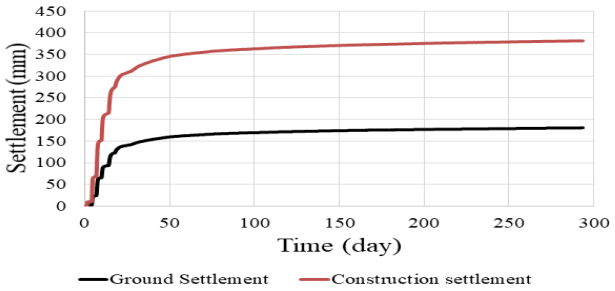

Fig. 11 Underground stress by centrifugal experiment

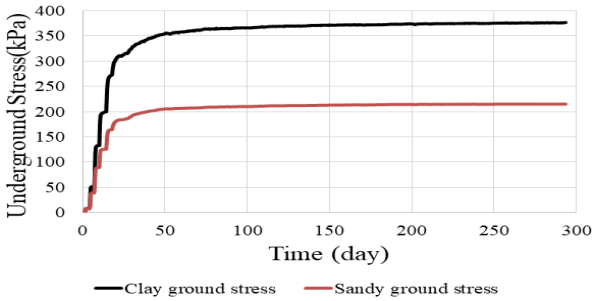

Fig. 12 Settlement by centrifugal experiment

Table 4 Law of similarity of centrifugal model test

Property	Centrifugal model	Real model
Volume	1	n^3
Stress	1	1
Time (consolidation)	1	n^2
Mass density	1	1
Displacement	1	n

the clay layer and the sandy soil layer. The displacement gauge was installed to measure the settlement in the structure and the substituted ground surface. The earth pressures with a measuring capacity of 490 kPa (MSP-5) and LVDT displacement CPT-25 & CPT-50 were used to measure the displacement and earth pressure data in the centrifugal model tests (Figs. 10(a)-10(b)). The earth pressure gauges were suitable for centrifugal model tests because of their small size and excellent durability. The CR1000 datalogger and Bluetooth wireless transmitter were used to monitor and collect data transmitted from the sensor installed in the chamber box.

Figs. 11 and 12 show the underground stress and settlement by a centrifugal experiment runed for 1.6 hour by case. The long-term settlement and underground stress can be obtained by calculating the similarity law. The values of the similarity ratio relationship between the properties of the real model and reduced model by centrifugal force are shown in Table 4. The calculated settlement was 67(n) times the measured value, and the actual medium stress was the measured value and the value of 1:1.

The results of the centrifugal model tests are shown in Table 5. Fig. 13 shows the underground stress distribution of the clay layer and sandy ground layer according to the particle size distribution condition. Fig. 14 shows the settlement amount in the structure and ground according to the particle size distribution condition. In the experimental results, the underground stress was the lowest at m=1.68

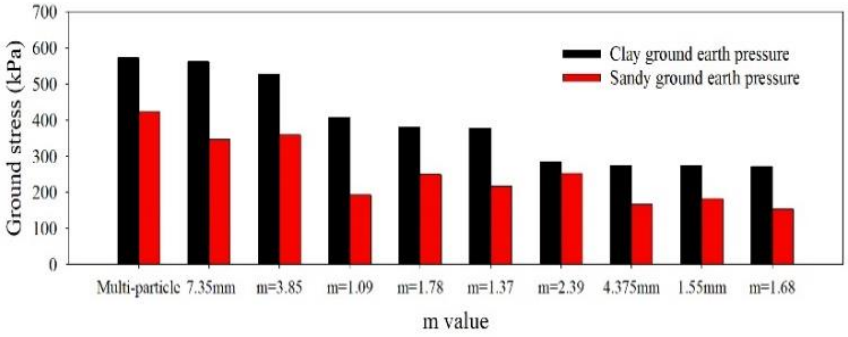

Fig. 13 Distribution of underground stress according to ground conditions

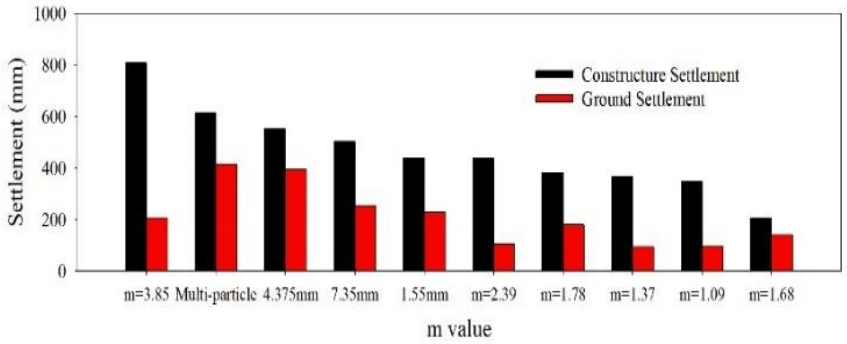

Fig. 14 Structure and ground settlement according to ground conditions

and highest in the multi-sized particle condition in the clay layer. The underground stress results were as follows: 1.55 mm, 4.375 mm, m=2.39, and m=1.37. In the clay layer, the underground stress of gap-graded particles m=1.68 was reduced by 45% compared with the multi-sized particles and reduced by 37% compared with the homogeneously sized particles of 1.55 mm. In the sandy layer, the underground stress was the lowest for the homogeneous particle size m=4.375 mm and the highest for the multi-sized particle condition. The underground stress results were m=1.68, m=1.55, m=1.09, and m=1.37.

The upper structure settlement for multi-sized particles and homogeneously sized particle was 4.375 mm larger than for gap-graded particles except when m=3.85. When m=1.68, the structure settlement decreased by 66% compared to the multi-sized particle condition and by 28.4% for the homogeneously sized particles of 1.55 mm. The ground settlement was the largest in the multi-sized particle condition, followed by a homogeneous particle size of 4.375 mm. The ground settlement was the lowest in the gap-grade size condition (m=1.37), followed by the gap-grade size condition (m=1.09). In the gap-grade particle size condition (m=1.37), the amount of ground settlement decreased by 77.4% compared to the multi-sized particle condition and by 75.2% in the homogeneous particle size condition (1.55 mm).

When interlocking between aggregates occurs in the gap-graded particle condition, the contact area increases, and the friction effect amplifies. It was confirmed that ground stress distribution and settlement were reduced. For the particle size condition, the gap-graded size performed well at m=1.68 and 1.37. Also, it can be seen that homogeneously sized particles of 1.55 mm (the smallest sized particles between the medium particles of 4.375 mm and the largest of 7.35 mm) have a greater effect on reducing the ground stress and settlement. but it also occurred largest settlement. so it is not best solution condition. There is a need to further determine the large to small particle aggregates' optimal ratio via a scaled-up test.

4.2 Performance evaluation of gap-graded grain ground through plate loading test

The concrete chamber dimensions were 1.5 × 1.5 × 1.5 m (width × length × depth). As shown in Fig. 15, earth pressure sensors were installed at 200 mm intervals from the loading plate center to measure the gap-graded aggregate ground stress distribution. The plate loading test was conducted using a 30 mm thick, 300 mm diameter loading plate and 30 tons capacity hydraulic cylinder (HD-317). Three particle distribution conditions were considered. The main and largest aggregate particle size was 13 mm, the main and largest aggregate size was 19 mm, with 13 mm and 19 mm gap-graded distribution, respectively. The mixing ratios for each aggregate are shown in Table 6. The ground was formed by placing aggregates in layers at 300 mm intervals and compacting the ground for 10 min with a compactor. The loading plate was 30 cm wide, and the load was applied in 10 steps until it reached 1700 kPa. Every step converged sufficiently until the next load.

In Fig. 17, through sieve analysis, the particle size's

Table 5 Results of centrifugal model tests

m value	Clay layer (kPa)	Sandy layer (kPa)	Ground settlement (mm)	Structure settlement (mm)
m=1.09	407.07	192.31	98.49	349.00
m=1.37	377.26	215.84	93.80	366.96
m=1.68	271.15	167.60	141.37	208.30
m=1.78	380.89	249.87	181.57	381.70
m=2.39	284.98	251.93	106.53	436.96
m=3.85	527.99	358.92	212.39	809.56
m=1, 1.55 mm	260.37	146.22	377.88	1054.92
m=1, 4.375 mm	274.59	182.11	230.48	439.32
m=1, 7.35 mm	561.92	406.72	396.97	786.6
Multi-sized particles	571.76	421.6	414.86	613.50

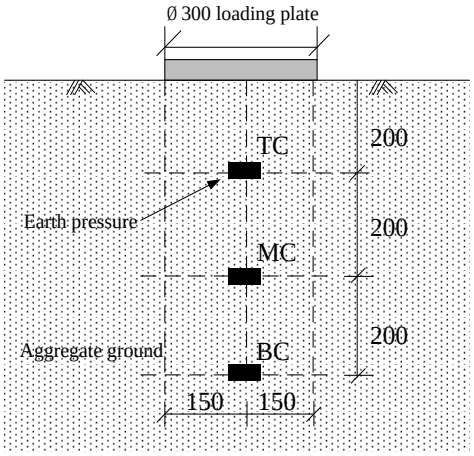

Fig. 15 Cross-section of chamber

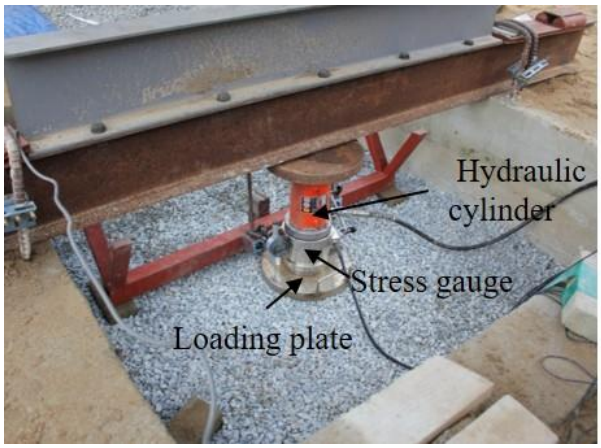

Fig. 16 Plate loading test

passing rate was graphed, and the uniformity coefficient and the curvature coefficient were obtained in Table 7. The data logger measured the displacement and earth pressure generated by increasing load and the ground stress transmitted from the earth pressure to each soil strata.

The Boussinesq equation for calculating the stress in the ground due to a concentrated load is as follows. The Boussinesq equation is used to determine the increment of vertical stress that occurs below the foundation's center under a circular distribution load (Ukritchon *et al*. 2016). If the loading surface radius is B/2, and the load is uniformly

Table 6 Composition of gap-graded aggregates

Aggregate size	Ground composition
13 mm aggregate	The largest particle size 13 mm aggregate
19 mm aggregate	The largest particle size 19 mm aggregate
13 mm & 19 mm aggregate	40% of 13 mm aggregate & 60% of 19 mm aggregate

Table 7 Aggregate type classification by USCS

Aggregate size	Cu	Cg	USCS*
13 mm	1.83	1.06	GP*
19 mm	2.27	1.08	GP
13 mm & 19 mm	1.98	0.98	GP

*GP: Poorly graded gavel

*USCS: Unified soil classification system

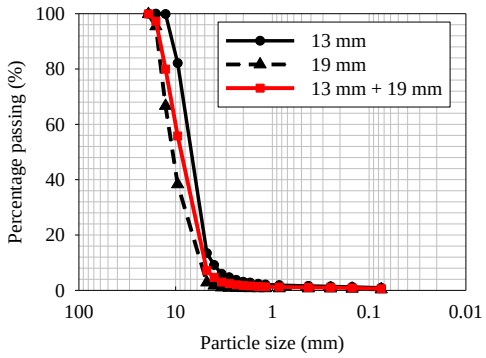

Fig. 17 Percentage passing by aggregate particle size

distributed, the soil stress changes with depth, as shown in Fig. 18. The load on a small area can be assumed to be a point load and expressed as q0rdθdr to find the stress increment at depth z below the loading area's center. The total stress increment caused by the loading area can be obtained by integration, as shown in Eq. (2).

$$\Delta\sigma = \int d\sigma = \int_{\theta=0}^{\theta=2\pi}\int_{\gamma=0}^{\gamma=B/2} \frac{3(q_0\gamma d\theta d\gamma}{2\pi z^2[1+\left(\frac{\gamma}{z}\right)^2]^{\frac{5}{2}}} = q_0\left\{1-\frac{1}{[1+(\frac{B}{2z})^2]^{\frac{3}{2}}}\right\} \quad (2)$$

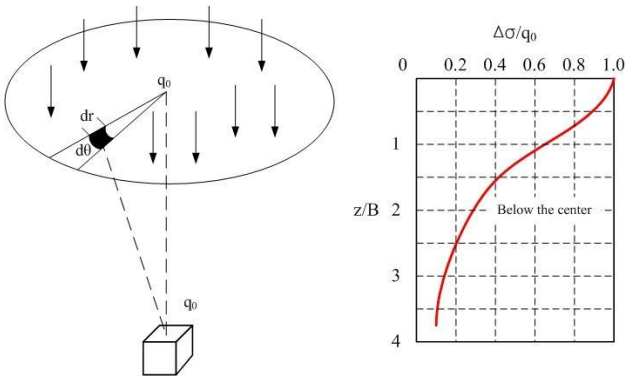

Fig. 18 Increase of vertical stress due to circular loading

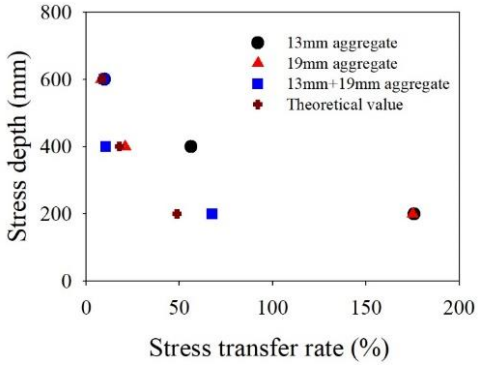

Fig. 19 Depth according to underground stress distribution

Fig. 19 shows the depth corresponding to the stress reduction below the center of the loading area derived from the ground condition under plate-loading tests. The soil pressure gauge readings were transferred to a data logger and recorded in real-time. After the load reached 1700 kPa, the ground stress transmitted to earth pressure gauges in each stratum located 200 mm apart. The earth pressure is converted into the stress transfer rate and compared for each ground condition. In addition, the depth under the center was calculated based on Boussinesq's equation, and the measured earth pressure for each depth was converted into a transmission rate. As the ground stress transfer rate rapidly decreased from the top with the ground's depth, the stress-transfer rate rapidly decreased as the depth increased. The stress taken from the plate loading test was substituted into Boussinesq's formula to compare the stress transfer rate with the experimental data. The stress transfer rate exceeded 100% due to the self-loading action of the ground aggregate.

The results are summarized in Table 8. The differences in the stress transfer rate obtained by the plate loading test and the theoretical calculation in the 13 mm aggregated ground were 127.15% at 200 mm depth, 38.29% at 400 mm, and 1.30% at 600 mm. The differences in the 19-mm aggregated ground were 126.27% at 200 mm depth, 2.98% at 400 mm, and 0.58% at 600 mm. The differences in the 13 mm and 19 mm aggregated grounds were 18.82% at 200 mm depth, 7.47% at 400 mm, and 0.91% at 600 mm. In evaluating the plate loading test's underground conditions, in the case of 13 mm and 19 mm sized aggregate

Table 8 Underground stress distribution results

Ground condition	Stress transfer rate with depth		
Particle size	200 mm depth	400 mm depth	600 mm depth
13 mm	175.95%	56.20%	9.99%
19 mm	175.07%	20.89%	8.11%
13 mm & 19 mm	67.62%	10.44%	9.6%
Theoretical result	48.8%	17.91%	8.69%

distribution the results showed larger stress transfer than the theoretical value, and for the gap-graded aggregate distribution, the results showed the smallest stress transfer and were closest with the theoretical value. Based on the experimental results, the closer they were to the gap-graded particle size condition, the greater the jamming effect due to interlocking, and the smaller the stress transfer area and the stress limit depth.

5. Conclusions

It can be expected that strong ground has a good particle size distribution. However, even if the particle size distribution is poor, the ground's strength can be significant in the gap-graded particle condition. In this study, the characteristics of the ground composed with gap-graded particles were investigated. Based on the numerical analysis and the centrifugal model tests, the gap-graded particle size ratio with the best performance was determined as m=1.37.

The uniaxial stress for the gap-graded particles was much higher than for the multi-sized particle distribution. The granular size composition showing the maximum uniaxial compressive strength is a combination of 7.35 mm and 5.175 mm particles with a gap-graded ratio of m = 1.42.

The shallow ground simulation results showed the highest ground strength at m=1.37 for the gap-graded particle size distributions, homogeneously sized particles, and multi-sized particles. The results showed high stress dispersion because of the interlocking effect.

In the centrifugal-model test and shallow-basis-simulation results, the specific gap-graded particle size conditions outperformed homogeneously sized particles, which outperformed particles with multiple sizes. This pattern was consistently observed. Numerical analysis and centrifugal testing showed that a gap-graded particle size ratio of m=1.37 showed the best performance.

In evaluating ground stress transfer through plate loading tests, the stress transfer rate was closest to the theoretical value for the 13 mm and 19 mm aggregate soils, and the ground stress distribution effect was superior to other conditions. The closer the ground particle size distribution is to the gap-graded particle size condition, the more interlocking effect caused by the interlocking and the smaller the stress limit depth.

Gap-graded aggregates rearrange themselves systemically from loose soil to dense soil when loading is applied. If the gap is reduced uniformly, the interlocking effect is exerted due to the particles' interlocking effect. Due to this action, the gap-graded granular ground settlement is small, and the bearing capacity is enhanced.

Acknowledgments

This work was supported by the National Research Foundation of Korea (NRF) grant funded by the Korean government (MSIT) (No. 2019R1A2B5B01069992).

References

Alias, R., Kasa, A. and Taha, M.R. (2014), "Particle size effect on shear strength of granular materials in direct shear test", *World Acad. Sci. Eng. Technol.*, *Int. J. Civ. Environ. Struct. Construct. Architect. Eng.*, **8**(11), 1093-1096.

Cho, G.C., Dodds, J. and Santamarina, J.C. (2006), "Particle shape effects on packing density, stiffness, and strength: Natural and crushed sands", *J. Geotech. Geoenviron. Eng.*, 591-602. https://doi.org/10.1061/(ASCE)10900241(2006)132:5(591).

Itasca Consulting Group Inc. (1999), *PFC2D Particle Flow Code in 2 Dimensions*, *Minneapolis: Itasca*.

Kamura, J.J. and Hayano, K. (2016), "Importance of particle shape on stress-strain behavior of crushed stone-sand mixtures", *Geomech. Eng.*, **10**(4), 455-470. https://doi.org/10.12989/gae.2016.10.4.455.

Nikadat, N. and Marji, M.F. (2016), "Analysis of stress distribution around tunnels by hybridized FSM and DDM considering the influences of joints parameters", *Geomech. Eng.*, **11**(2), 269-288. https://doi.org/10.12989/gae.2016.11.2.269.

Oda, M. (1977), "Co-ordination number and its relation to shear strength of granular material", *Japan. Soc. Soil Mech. Found. Eng.*, **17**(2), 29-42. https://doi.org/10.3208/sandf1972.17.2_29.

Saride, S., Pradhan, S., Sitharam, T.G. and Pippala A.J. (2013), "Numerical analysis of geocell reinforced ballast overlying soft clay subgrade", *Geomech. Eng.*, **5**(3), 263-281. https://doi.org/10.12989/gae.2013.5.3.263.

Shen, D.H., Kuo, M.F., Du, J.C., (2005), "Properties of gap-aggregate gradation asphalt mixture and permanent deformation", *Construct. Build. Mater.*, **19**, 147-153. https://doi.org/10.1016/j.conbuildmat.2004.05.005.

Siemens, A.O.N. and Hecke, M.V. (2010), "Jamming: A simple Introduction", *PhtsicaA*, **389**, 4255-4264. https://doi.org/10.1016/j.physa.2010.02.027.

Takao, U., Takashi, M. and Yasuo, Y., (2011), "Effect of particle size ratio and volume fraction on shear strength of binary granular mixture", *Granular Matter*, **6**(13), 731-742. https://doi.org/10.1007/s10035-011-0292-1.

Ukritchon, B., Faustino, J.C. and Keawsawasvong, F.S. (2016), "Numerical investigations of pile load distribution in pile group foundation subjected to vertical load and large moment", *Geomech. Eng.*, **10**(5), 577-598. https://doi.org/10.12989/gae.2016.10.5.577.

Vallejo, L.E. and Chik, Z. (2009), "Fractal and laboratory analyses of the crushing and abrasion of granular materials", *Geomech. Eng.*, **1**(4), 323-335. https://doi.org/10.12989/gae.2009.1.4.323.

Viggiani, G., Küntz, M. and Desrues, J. (2001), "An experimental investigation of the relationships between grain size distribution and shear banding in sand", *Part Lecture Notes Physics Book Series*, **568**, 111-127. https://doi.org/10.1007/s10035-011-0292-1.

Wang, Z., Ruiken, A., Jacobs, F. and Ziegler, M., (2014), "A new suggestion for determining 2D porosities in DEM studies", *Geomech. Eng.*, **7**(6), 665-678. https://doi.org/10.12989/gae.2014.7.6.665.

Xin, Z.H., Moon, J.H., Kim, L.S., Kim, G.B. and Kim, Y.U. (2016), "Effect of arbitrarily manipulated gap-graded granular particles on reinforcing foundation soil", *Geomech. Eng.*, **17**(5), 439-444.

Yagiz, S. (2001), "Brief note on the influence of shape and percentage of gravel on the shear strength of sand and gravel mixtures", *B. Eng. Geolog. Environ.*, **60**(4), 321-323. https://doi.org/10.1007/s100640100122.

IC